Colloids and Surfaces A: Physicochemical and Engineering Aspects 657 (2023) 130561

Contents lists available at ScienceDirect

Colloids and Surfaces A: Physicochemical and Engineering Aspects

journal homepage: www.elsevier.com/locate/colsurfa

Facile approach to fabricate a high-performance superhydrophobic PS/OTS modified SS mesh for oil-water separation

Rajaram S. Sutar [a], Sanjay S. Latthe [b,*], Nilam B. Gharge [a], Pradip P. Gaikwad [a], Akshay R. Jundle [a], Sagar S. Ingole [a], Rutuja A. Ekunde [a], Saravanan Nagappan [c], Kang Hyun Park [c], Appasaheb K. Bhosale [a], Shanhu Liu [d,*]

[a] Self-Cleaning Research Laboratory, Department of Physics, Raje Ramrao College, Jath, Dist: Sangli – 416404, (Affiliated to Shivaji University, Kolhapur), Maharashtra, India

[b] Self-cleaning Research Laboratory, Department of Physics, Vivekanand College, Kolhapur (Autonomous) – 416 003, (Affiliated to Shivaji University Kolhapur), Maharashtra, India

[c] Department of Chemistry, Chemistry Institute for Functional Materials, Pusan National University, Busandaehak-ro 63 beon-gil, Geumjeong-Gu, Busan 46241, Republic of Korea

[d] Henan Key Laboratory of Polyoxometalate Chemistry, Henan Joint International Research Laboratory of Environmental Pollution Control Materials, College of Chemistry and Chemical Engineering, Henan University, Kaifeng 475004, PR China

GRAPHICAL ABSTRACT

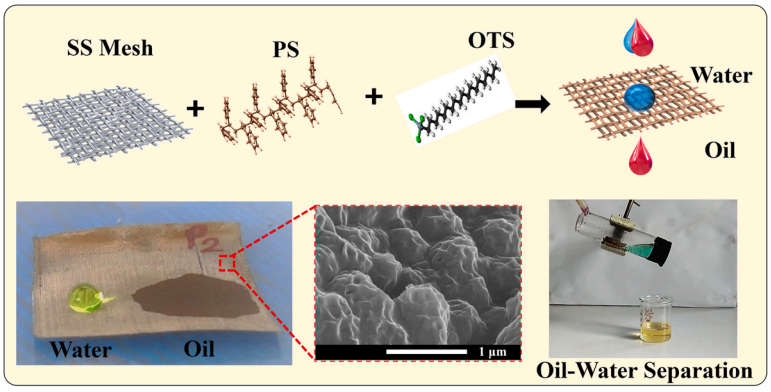

ARTICLE INFO

Keywords:
Oil-water separation
Stainless steel mesh
Superhydrophobic
Superoleophilic

ABSTRACT

Special wetting materials have been used for the oil and water separation due to their different interfacial attraction of oil and water. Herein, we successfully fabricated superhydrophobic coatings on stainless steel (SS) mesh by depositing successive layers of polystyrene (PS) and octadecyltrichlorosilane (OTS) through the dip-coating method. The as-prepared coating showed a water contact angle (WCA) of 157.5 ± 2°, a rolling angle of 6 ± 2° and an oil contact angle (OCA) of around 0°. The surface microstructure analysis of the coating revealed a regular pattern of microscale bumps with nanoscale folds on it, both of which improve the overall superhydrophobicity of the surface. The capacity of coatings to separate oil and water was examined by

* Corresponding authors.
E-mail addresses: latthes@gmail.com (S.S. Latthe), liushanhu@vip.henu.edu.cn (S. Liu).

https://doi.org/10.1016/j.colsurfa.2022.130561
Received 12 September 2022; Received in revised form 26 October 2022; Accepted 10 November 2022
Available online 14 November 2022

employing a variety of mixtures of oil and water, including petrol, diesel, kerosene, vegetable oil, and coconut oil. In case of low viscosity oil, the coated mesh demonstrated separation effectiveness of more than 97% and on the other hand, high viscosity oil demonstrated just 89% efficiency. Low viscosity oils showed a greater permeation flux through the mesh than extremely viscous oil. The mechanical strength of the coating was examined using bending, twisting, adhesive tape testing, sandpaper abrasion tests, and the findings indicated that coated mesh had exceptional mechanical resilience. In addition, the developed superhydrophobic mesh demonstrated excellent thermal stability and self-cleaning properties. Therefore, this superhydrophobic/superoleophilic mesh has a significant deal of application potential in practical.

1. Introduction

Oil spills and industrial effluents inflict significant harm to the ecosystems of the seas, human health, and the surrounding environment [1,2]. The safe and responsible disposal of wastewater containing oil has been shown to be a challenging problem on a global scale. Many approaches have been used for the treatment of oil-water pollution, including oil skimmers, filtration, oil-absorbing materials, magnetic separations, centrifugal machine, flotation technologies, and combustion [3–5]. Traditional methods have various drawbacks, including limited separation efficiency, time consumption, cost-effectiveness, and the generation of secondary pollutants [6–8]. Therefore, cutting-edge technologies are an absolute necessity for the disposal of oily wastewater and the protection of the environment. Many efforts have been reported in the fabrication of separation membranes with controlled surface wetting property [9,10]. The utilization of bio-inspired superhydrophobic materials in oil-water separation processes is a popular area of study due to its high water repellency and ability to allow oil to enter in it [4,11,12]. Therefore, superhydrophobic materials have been added to commercially available cotton textiles, 3D porous materials, different polymer membranes, filter papers, and metal meshes for considerable oil-water separation [13,14]. Chemical etching [15,16], spray deposition [17,18], dip coating [19], hydrothermal method [20], sol-gel processing [21,22], chemical vapor deposition [23], electrospinning [24,25], and layer by layer [26] methods have been used for modification of porous surfaces. Among these, dip-coating is a quick and effective method of producing bulky, intricately formed products [27]. Metal meshes have sparked a lot of attention since they are long-lasting, reusable, and may be used in industry [2,23]. Porous materials can absorb or filter liquids, and when their surface structure is adjusted with a specific wettability material, they can help separate oil or water from oil-water mixtures [28,29]. Numerous types of porous metal meshes, including those constructed of nickel, copper, and stainless steel (SS), among other materials were used for oil-water separation [30–33]. Among them, SS meshes have found widespread use for oil-water separation owing to their high electrical and electrothermal capabilities as well as their superior resistance to thermal shock [33].

OTS has been used to tune the surface wettability of porous substrates so that oil and water can be effectively separated. The OTS has low surface energy, hence it improves the hydrophobicity of the rough surface and also shows high oil absorption capacity [35,36]. Li et al. [34] recently made superhydrophobic SS mesh by spraying it with a mixture of OTS-modified SiO_2 nanoparticles and waterborne PU. This superhydrophobic mesh was able to separate a mixture of kerosene and water at a rate of 98.3%. Latthe et al. [27] created a superhydrophobic surface by varying the concentration of OTS in PS solution and the number of dipping cycles. At first, they prepared a homogenous solution containing PS and OTS using tetrahydrofuran (THF) as a solvent. The pre-cleaned glass substrate was dip-coated (4 times) on the homogenous solution and air-dried to get a superhydrophobic surface with a contact angle of 154 ± 2°. Ke et al. [37] have built a superhydrophobic and superoleophilic sponge by immersing it in OTS solution. This kind of sponge has shown an absorption capacity of 42–68 times more than the mass of the sponge for toluene, light oil, and methyl silicone oil. Even after being put through 50 separation cycles, this adsorption capacity remained the same. Liang et al. [38] modified a polyurethane sponge by immersing in an OTS solution for oil-water separation. Cheng et al. [24] used coaxial electrospinning with PVDF solution as a lumen solution and reactive silicon-containing monomers as the outer solution to generate superhydrophobic nanofiber membranes with hierarchical micro nano-scale morphology. The outstanding separation efficiency of 99.6% is achieved with the as-prepared asymmetric composite membrane, which has an extremely rapid permeation flux. They show a water-in-n-octane permeation flux of 17331 L/(m^2h) and retain 88% of their original permeance after 20 cycles of operation [24]. Rasouli et al. [13] briefly reviewed the various aspects of fabrication of superhydrophobic/superoleophilic membranes having mesh, films, and porous substrates for efficient oil-water separation applications. In order to modify the surface energy of superhydrophobic/superoleophilic membranes, it is usual practice to use low surface energy chemicals such as fatty acids, thiols, silanes, polymers based on polyethylene, and carbon nanotubes [13]. These membranes have > 99% oil separation efficiency in oil-water combinations.

In this research work, a layer of PS was first applied on SS mesh using a dip coating process, followed by an OTS dip layer to achieve superhydrophobicity. The dip coating cycles were consequently carried out by dip and dry in both PS in THF and OTS in hexane. The surface structure of a red rose petal was obtained on SS mesh. SEM and EDS were used to describe the surface morphology and chemical composition, respectively. The gravity-driven oil-water separation technique was used to determine the oil-water separation efficiency and permeation flux using a custom-made setup. The mechanical durability of superhydrophobic mesh was evaluated using adhesive tape tests, sandpaper abrasion tests, bending, twisting, and folding tests. We have achieved the contact angles of 157.5 ± 2° for OPS-2 as well as 154 ± 2° for OPS-3 in superhydrophobic range and a comparable contact angle of 148.5 ± 2° for OPS-1. The stable and robust self-cleaning coating was produced by this method as compared with the reported methods.

2. Experimental section

2.1. Materials

Polystyrene (PS) having average molecular weight ~ 280,000 and octadecyltrichlorosilane (OTS) were obtained from Sigma Aldrich, St. Louis, MO, USA. Tetrahydrofuran (THF) and hexane were purchased from Spectrochem, Mumbai, India. Stainless steel (SS) mesh with pore sizes of about 50 μm was obtained from Shanghai Titan Technology Co. Ltd. China. The petrol, diesel, kerosene (from Bharat Petroleum Corporation Limited, India), vegetable oil (from Garud, India), and coconut oil (from Parachute Advanced, India) were purchased.

2.2. Preparation of superhydrophobic mesh

In the beginning, 0.4 g of PS was dissolved into 16 mL of THF under vigorous stirring. Simultaneously, a 0.8 mL OTS was diluted in 16 mL hexane by stirring for 30 mins in a separate beaker. Prior to use, SS mesh was cut into squares of 2 cm × 2 cm and then ultrasonically cleaned in ethanol and purified water. At first, the cleaned mesh was submerged in PS solution for 1 min, after which it was pulled out at a speed of around

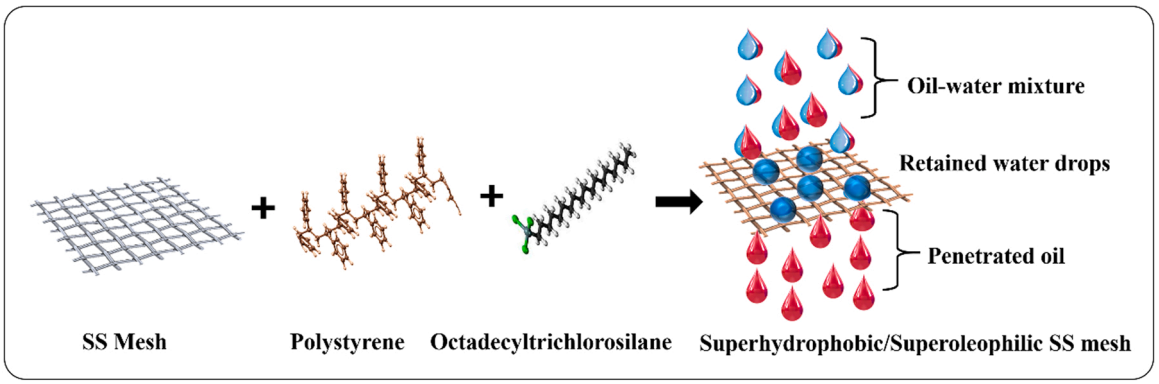

Fig. 1. Schematic of preparation of superhydrophobic SS mesh.

100 mm s^{-1}. The PS-coated mesh was first allowed to dry at room temperature, then dipped for 1 min in a beaker that had a solution of OTS in hexane, after which it was taken out, and finally allowed to dry at room temperature. An alternate PS and OTS coatings were applied back-to-back ten times. Finally, all solvents were evaporated during the course of a 1 h drying period at 100 °C. As a result, the amount of OTS used in this coating procedure was changed from 1.6 to 2.4 mL. OPS-1, OPS-2, and OPS-3 signify 0.8, 1.6, and 2.4 mL of OTS coated SS mesh, respectively. Fig. 1 depicts the creation of a superhydrophobic mesh.

2.3. Characterizations

The surface morphology of the produced coatings was investigated using Scanning Electron Microscopy (SEM, JEOL, JSM-7610 F, Tokyo, Japan). Chemical examination of the coating was carried out using Energy Dispersive Spectroscopy (EDS, Hitachi, Ltd., Tokyo, Japan) in order to determine the elemental percentage of the coating. Fourier-transform infrared spectroscopy (FTIR, Magna-IR 560, Nicolet) was used to analyse the chemical composition of the samples. Contact Angle Meter (HO-IAD-CAM-01, Holmarc Opto-Mechatronics Pvt. Ltd., Kochi, India) was used to measure the water/oil contact angle and slide angle of prepared coatings. Using a micro-syringe of the contact angle meter ~10 μL sized water droplet was placed on the coated mesh. The value of water contact angles and sliding angles were measured at five different places of coated mesh and reported an average value of them. The capacity of superhydrophobic mesh to separate oil from water was tested using a custom-made oil-water separation apparatus. In the middle of the bottle cap, a hole with a diameter of 2 cm was drilled using a drill and the superhydrophobic OPS-2 mesh was then bonded inside the bottle cap over the circular hole using glue. The bottom of the bottle was cut off and then clamped at an angle that was roughly 45°. In a typical experiment, the oil-water combination was made by adding 10 mL of water into 10 mL of oil. The different type of oils including petrol, diesel, kerosene, coconut and vegetable oil were used to produce oil-water mixture. Mechanical durability of superhydrophobic mesh was evaluated using bending, twisting, adhesive tape testing, and sandpaper abrasion. In order to execute the adhesive tape peeling test, tape with a 4 N/m adhesive strength was affixed on superhydrophobic OPS-2 mesh and eventually peeled off. In order to determine the level of mechanical strength possessed by superhydrophobic mesh, OPS-2 mesh was laid out on sandpaper (grit no. 320), a metal disc weighing 100 g was put on top of the mesh, and the mesh was pulled for 5 cm to complete one abrasion cycle. The thermal stability of the produced superhydrophobic OPS-2 mesh was evaluated by heating it for 1 h in a hot air oven at 150 °C

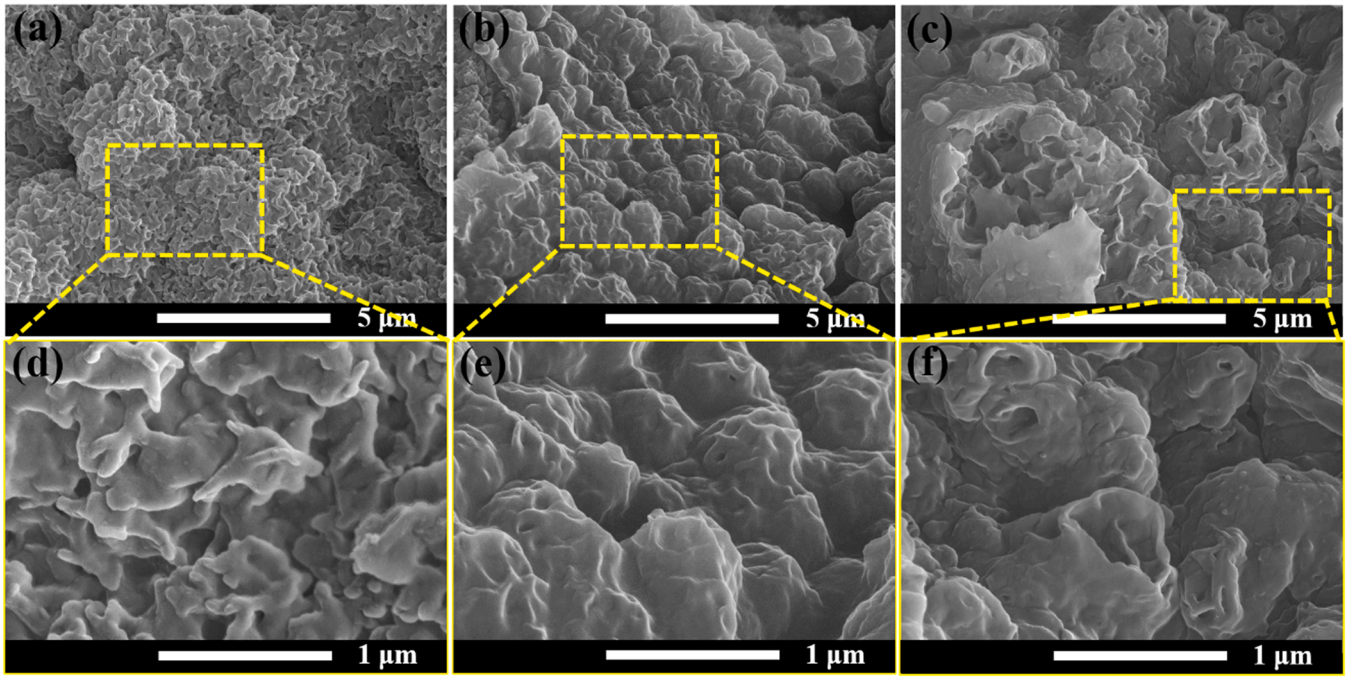

Fig. 2. SEM images of OPS-1, OPS-2, and OPS-3 mesh at (a-c) low and (d-f) high magnifications, respectively.

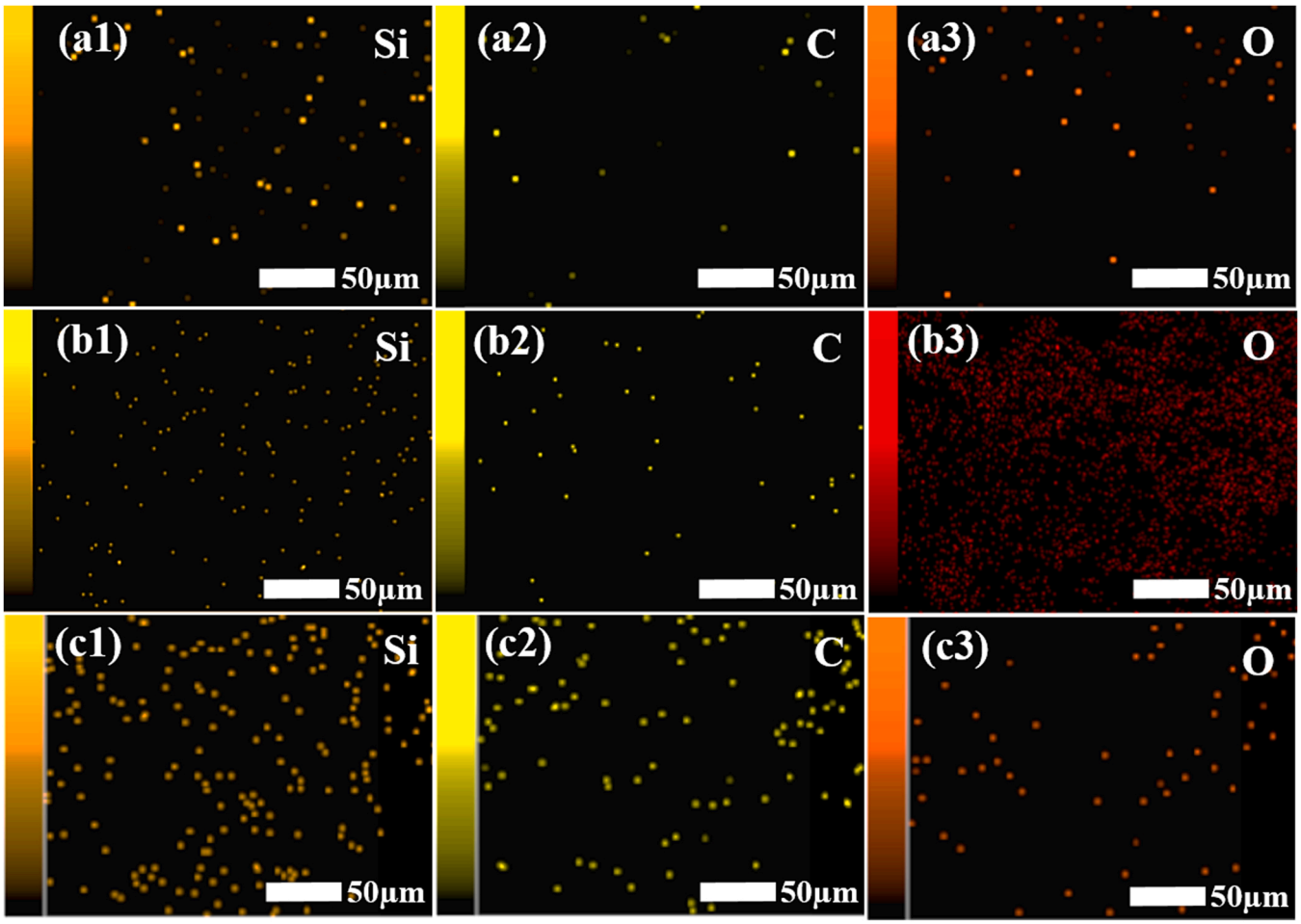

Fig. 3. EDS mapping images of OPS-1 (a1-a3), OPS-2 (b1-b3) and OPS-3 (c1-c3) mesh.

and 200 °C. The self-cleaning ability of superhydrophobic OPS-2 mesh was investigated by the muddy water, fine particles of ash and wood charcoal as dust containments. The muddy water was produced by combining 5 g of tiny dirt particles with 20 mL of the water and then dumping the mixture onto an angled superhydrophobic mesh. The dispersion of ash in water was prepared by adding 5 g of ash in the 20 mL of water and mixed well by glass rod. The superhydrophobic OPS-2 mesh was immersed into it. The fine particles of wood charcoal dispersed on inclined superhydrophobic OPS-2 mesh and water jet dropped on it.

3. Results and discussion

3.1. Surface morphology and chemical composition

Fig. 2(a-f) depicts the surface morphology of meshes after being treated with varying doses of OTS. At low OTS concentrations, ten successive coating layers of PS and OTS create a rougher surface with nanoscale folds, as seen in Fig. 2(a). The enlarged view shows that there is a regular micro and nanoscale rough texture, which is essential for improving hydrophobicity and can be observed in Fig. 2(d). Surprisingly, regular shaped bumps emerged after raising the OTS concentration by twofold, as illustrated in Fig. 2(b). These regular-shaped bumps seem to be a regular arrangement of micropapillae on a red rose petal. Fig. 2(e) illustrates how each bump has a few nanoscale folds on its top surface. As a consequence of these microscaled bumps and nanoscaled folds on top of bumps, the superhydrophobicity of the surface might have increased. As the concentration of OTS was raised three times,

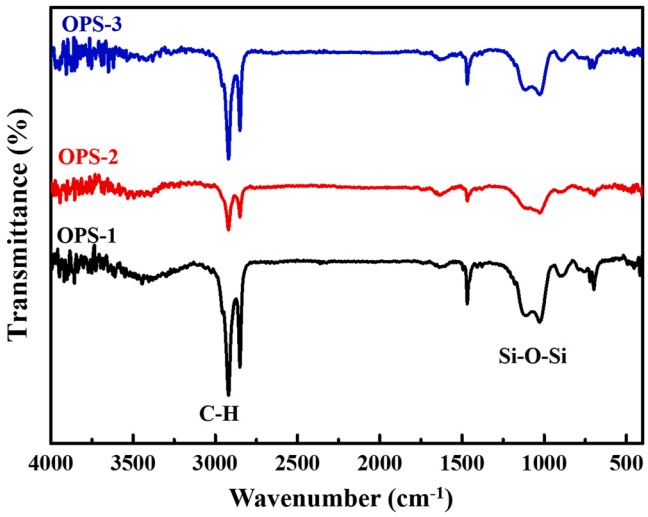

Fig. 4. FTIR spectra of prepared OPS-1, OPS-2 and OPS-3 mesh.

larger bumps developed, which were broken following heat treatment due to solvent evaporation (see Fig. 2c). The greater the size of the bumps, the more they affect the surface's roughness and wettability (Fig. 2f). The difference in the surface structure may be due to the formation of an aggregate particles by the deposition PS particles on SS mesh. This can produce a hierarchical rough surface morphology which

Table 1
Elemental ratio of C, O, and Si occurred in the prepared superhydrophobic coating.

Sample	Si -K		C-K		O-K	
	Mass%	Atom%	Mass%	Atom%	Mass%	Atom%
OPS-1	2.28	1.29	5.97	7.87	91.75	90.84
OPS-2	6.43	3.65	9.48	12.58	84.09	83.77
OPS-3	16.35	9.65	10.68	14.74	72.97	75.61

further attracted together by following OTS coating on the surface. OTS can form a thin hydrophobic layer on the surface of PS particles. The subsequent hydrolysis and condensation of OTS plays an important role in the surface morphology. The formation nanosheets after hydrolysis and condensation of OTS was reported earlier [27,39]. The formation of Si-O-Si bonds were also confirmed from FT-IR studies which supports the hydrolysis and condensation of OTS (Fig. 4). The SS mesh substrate can produce a rough surface morphology by applying consecutive dip-coating cycles for 10 times. The surface morphology can further produce a layered structure by increasing the coating cycles. The SEM images clearly depicts that, based on the dip coating cycles, the surface morphology can be tuned from regular micro and nanoscale rough texture to layered larger bumps due to formation of more curvy OTS nanosheets on the PS coated mesh.

EDS spectra was used for chemical investigation of the coating. In the EDS spectra three elements are detected such as carbon (C), oxygen (O), and silicon (Si) as shown in Fig.S1. The mass and atomic percentages of the elements C, O, and Si that were present in the coating are detailed in Table 1. A higher proportion of C was produced as a result of the presence of polystyrene as well as the alkyl chain in OTS. The Si is attributed to OTS. The presence of C and Si implies that the coating material covers the mesh surface consistently. Fig. 3 illustrate that the elemental mapping images of coatings. The uniform distribution of Si, C, and O element at coating surface were seen in the elemental mapping images of OPS-1, OPS-2 and OPS-3 coating, implying the PS and OTS layers homogeneously deposited on mesh.

To confirm the bonding between PS and OTS on coating surface the FTIR analysis was carried out. As shown in Fig. 4, the FTIR spectra of OPS-1, OPS-2 and OPS-3 coated mesh has the strong two peaks at 2922 cm^{-1} and 2852 cm^{-1} are attributed to C–H asymmetric stretching vibrations and symmetric stretching vibrations, respectively indicating that presence of alkyl group of OTS chain. The peaks at 1051 cm^{-1} and 796 cm^{-1} are indicating that existence of Si-O-Si asymmetric and symmetric starching vibration, respectively. The existence of Si, C and O along with C-H and Si-O-Si bonding concludes that the PS and OTS made strong bonding in between and uniformly presence on the coating surface.

3.2. Wettability of coated mesh

Water and oil contact angle measurements were used to assess the wetting behaviour of coated meshes. The coated mesh demonstrated simultaneously superhydrophobic and superoleophilic and qualities as a result of its dual scale roughness in addition to its low surface energy OTS. The oil-water separation application of mesh requires both the superhydrophobic and the superoleophilic characteristics in order to be successful [40]. The relationship between surface roughness factor and surface wettability can be explained by Cassie-Baxter equation is written out as following form:

$$\text{Cos}\,\theta^* = f_1\,(\text{Cos}\,\theta + 1) - 1 \quad (1)$$

where, θ^* and θ are the apparent contact angle of a water droplet on a rough surface and a perfectly flat surface, respectively. f_1 is the fraction of solid substrate that comes into contact with the liquid. In this study, the WCA of uncoated mesh (θ) and superhydrophobic OPS-2 mesh (θ^*) were 84° and 157.5°, respectively. The WCA's were measured immediately after placing water drops on uncoated and superhydrophobic OPS-2 mesh. Using the above equation, the calculated value of f_1 is 0.06890. This implying that only 6.89% of the surface area was in direct contact with the water and 93.11% of the rough surface area was covered with the air. In the presence of a low concentration of OTS, the ten successive depositions of layer of PS and OTS revealed a WCA of 148.5 ± 2° (OPS-1). The WCA reached its maximum value of 157.5 ± 2°

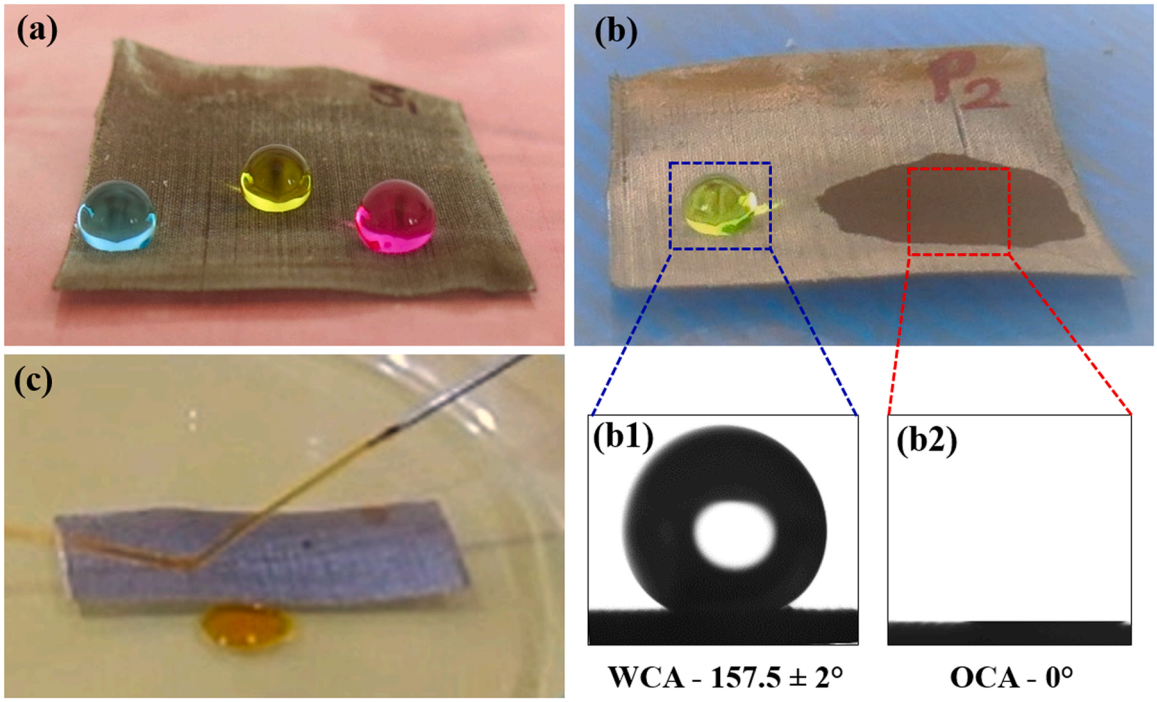

Fig. 5. (a) Colour water drops on OPS-2 mesh, (b) water and oil drop on OPS-2 mesh, (b1 and b2) digital image of water and oil on OPS-2 mesh, respectively, and (c) water jet impact test on OPS-2 mesh.

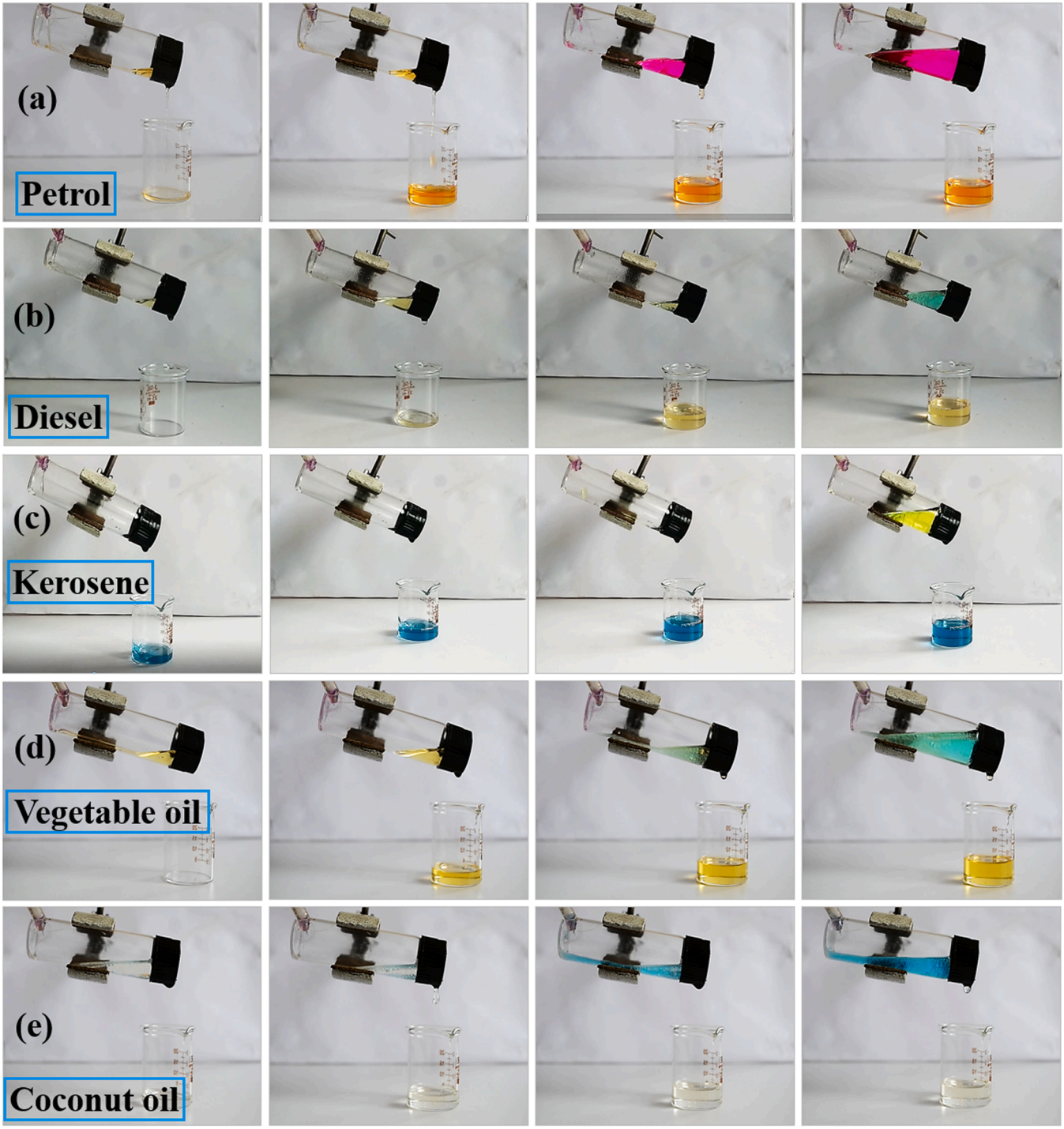

Fig. 6. The few screen snaps of oil-water separation process by OPS-2 mesh (a) petrol, (b) diesel, (c) kerosene, (d) vegetable and (e) coconut oil.

with sliding angle of 6 ± 2° (OPS-2) as the concentration of OTS rose in successive layered depositions of PS and OTS. The top of the surface has microscale bumps and nanoscale folds, which combine to generate hierarchical dual scale roughness. This dual scale roughness allows an air layer to get trapped, which in turn increases water repulsion. The colourful water droplets on the superhydrophobic OPS-2 mesh were visible in Fig. 5(a). When the concentration of OTS was increased later, the size of the bumps became larger, and the bumps fragmented after heat treatment. The broken bumps had an effect on the surface structure, and as a result, the WCA was reduced to 154 ± 2° (OPS-3). The OCA was also measured for the prepared coatings, and almost all of them revealed roughly 0° of OCA. A ball-like form was achieved by the drop of water, but the drop of oil entirely soaked up moisture from the OPS-2 mesh surface (Fig. 5b). The digital picture graphs of a water drop and an oil drop on OPS-2 mesh are presented in Fig. 5 (b1) and (b2), respectively. The effect of a water jet impact on OPS-2 mesh was used to test the wetting stability of the coating (Fig. 5c). The water jet was generated by a syringe with a capacity of 10 mL, and it constantly struck a predetermined location on the coating. The hit jet moved in the opposite direction from the place of impact once it had been disrupted. The coating passed the water jet impact test, which proves that it can withstand being repeatedly impacted by water. As a result, a

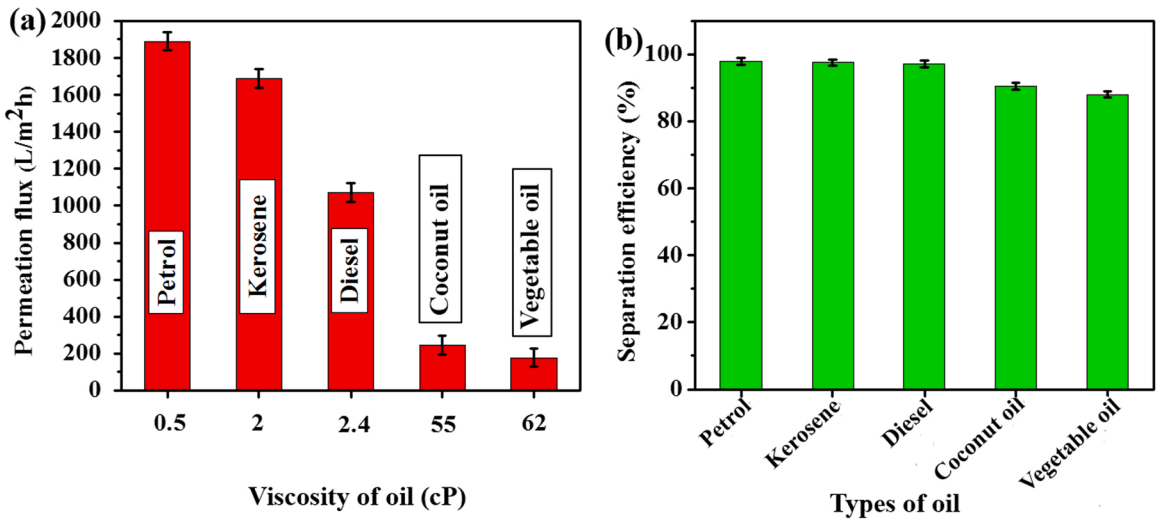

Fig. 7. (a) Permeation flux and (b) separation efficiency of OPS-2 mesh for different kind of oil-water mixture.

Table 2
Comparision between present work and previous reported literature.

Materials	Substrate	Separation efficiency (%)	Permeation Flux L/ (m^2h)	Ref.
NaOH/APS - PDMS	Copper mesh	98.89	11	[31]
APT nanorods and OTMS	SS mesh	99.4	106.7	[41]
Perfluorooctyltriethoxysilane	SS mesh	99.5	70	[44]
Dopamine hydrochloride, n-dodecyl mercaptan, and Tris(hydroxymethyl) aminomethane hydrochloride	Copper mesh	90	4507	[45]
Choline chloride, ethylene glycol, stearic acid	Copper mesh	99.82	1725	[46]
1-(chloromethyl)– 4-ethenyl-benzene, N, N-dimethyl dodecylamine, SiO_2 nanoparticles	SS mesh	99.8	15.65	[47]
Sodium sulfate anhydrous and copper chloride	Copper Mesh	90	4378	[48]
Hydrophobic SiO_2 nanoparticles and thermoplastic acrylic.	SS mesh	99.5	–	[49]
Sodium hydroxide and copper (II) chloride dehydrate	SS mesh	99.0	–	[50]
Lignin-coated cellulose nanocrystal, Polydimethylsiloxanes Poly-vinylidene fluoride and 1 H,1 H,2 H,2 H-perfluorooctyltrichlorosilane	SS mesh	94.5	–	[51]
PS/OTS	**SS mesh**	**97**	**1689.189**	**Present work**

superhydrophobic mesh that is capable of separating oil and water combination in flowing mode was created.

3.3. Oil-water separation

The oil-water separation experiment was carried out by using a setup that was specifically constructed for oil-water separation. Fig. 6(a-e) depicts the experimental setup for the oil-water separation process, along with screen shots of the oil-water separation process. The use of gravity alone was sufficient to distinguish oil from water in a combination of oil and water, which suggests that oil and water may be separated with very little effort [41]. Before using superhydrophobic mesh for oil-water separation, one must examine the permeation flux and separation efficiency [42]. The oil flow was calculated by dividing the total volume of permeated oil (V) by the product of the effective area of the mesh (S) and time (T) necessary for oil permeation [43]. At atmospheric pressure and room temperature, the permeation flux of different kinds of oil-water mixtures was worked out. The viscosity of the oil has an effect on the permeation flux; low viscous oil, such as petrol, has demonstrated a permeation flux of 1689.189 L/(m^2h), while high viscous oil, such as vegetable oil, has a permeation flux of 177.16 L/(m^2h). Fig. 7(a) shows the value of permeation flux for different viscosity of oil-water mixtures.

The separation efficiency (η) was estimated by comparing the volume of oil after (m) and before the separation of mixture [28]. The effectiveness of the separation efficiency for the different oil-water mixtures is shown in Fig. 7(b). The low viscosity oils penetrated rapidly through the mesh's porous structure and displayed separation efficiency greater than 97%. Over the course of more than 20 separation cycles, the superhydrophobic mesh maintained its effectiveness in the separation of these oils. Because of oil partly caught in the mesh, the separation efficiency of very viscous oils was less than 89%. As a result, the superhydrophobic mesh exhibited 8 separation cycles for high viscosity oil. Table 2 illustrates the comparison between present work and previous reported literature related to superhydrophobic/superoleophilic metal mesh.

3.4. Mechanical durability tests

In order to take an industrial approach, it is necessary to investigate the mechanical strength of superhydrophobic mesh. Recent research conducted by Varshney et al. [52] and Luo et al. [53] investigated the mechanical endurance of superhydrophobic mesh by bending, twisting, testing with adhesive tape, and abrasion testing with sandpaper. The

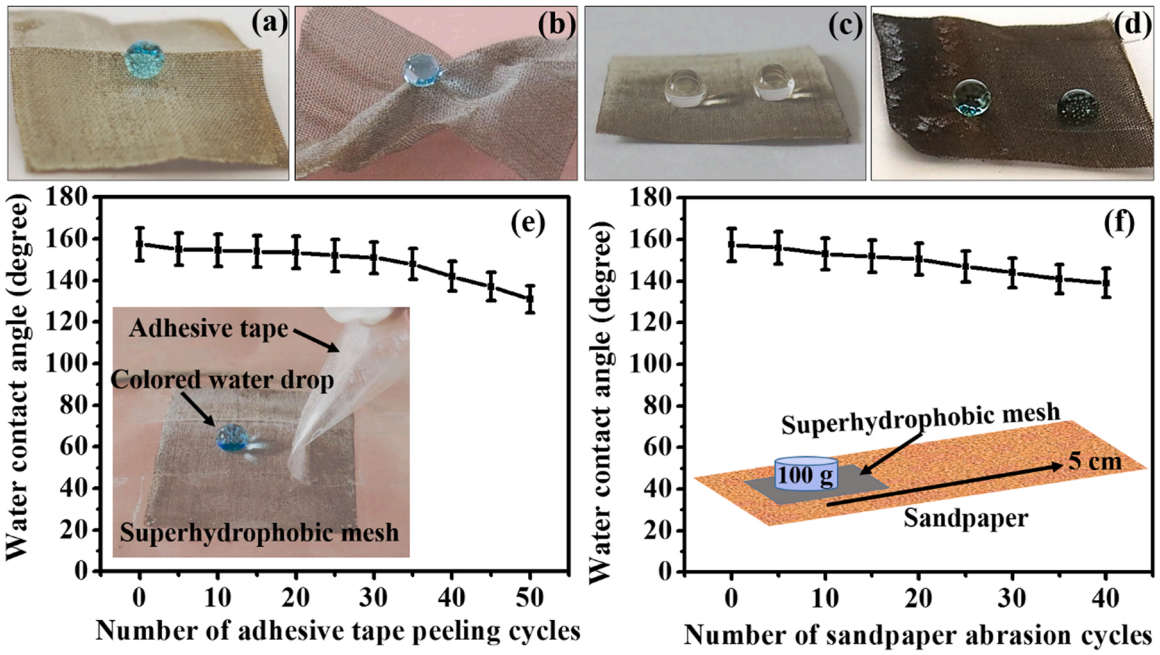

Fig. 8. Photographs of (a) folding, (b) twisting of OPS-2 mesh, (c) hot water drops on OPS-2 mesh, (d) photograph of OPS-2 mesh after heating, (e) variation of WCA with adhesive tape peeling cycles and in inset experiment setup of adhesive tape test, and (f) the results of sandpaper abrasion test and in inset schematic of sandpaper abrasion test.

degradation of WCA after mechanical durability testing was thoroughly investigated in this paper. It was discovered, after subjecting a superhydrophobic mesh to a variety of bending and twisting motions, that the superhydrophobicity of the mesh remained unchanged. The photographs of the superhydrophobic mesh being bent and twisted are shown in Fig. 8(a) and (b), respectively. For the purpose of the adhesive tape peeling test, tape was placed on superhydrophobic mesh (OPS-2) and then peeled off gradually (see inset of Fig. 8e). Immediately, the WCA was measured using a contact angle meter on the portion of the mesh that had been impacted by the tape. This tape peeling test was done multiple times until the superhydrophobicity subsided. The degradation of as a result of several tape peeling tests is seen in Fig. 8(e). During 20 cycles of adhesive tape testing, the superhydrophobicity of mesh was sustained with a WCA of 153.5 ± 2° and SA of 8 ± 2°. As the number of tape peeling cycles continued to increase, the water drop that was stuck to the mesh may have been detached from the hydrophobic substance, resulting in the disappearance of the surface structure of the coating. The WCA reached to 131.5 ± 2° after 50 rounds of the tape peeling test.

The sandpaper abrasion process is shown schematically in the inset of Fig. 8(f). One cycle of sandpaper abrasion test is defined as 5 cm dragging of mesh on sandpaper, and WCA was measured at the affected region of mesh after each cycle. The reduction in WCA value as a function of sandpaper abrasion cycles is seen in Fig. 8(f). Even after 20 cycles of sandpaper abrasion tests, the mesh still exhibited superhydrophobic characteristics with WCA of 150.5 ± 2° and SA of 7.5 ± 2°, indicating that the superhydrophobic material was effectively attached to the mesh. The mesh lost its superhydrophobic ability as the sandpaper abrasion cycles increased, confirming that the hierarchical structure of the coated surface vanished. The mesh WCA was lowered to 139° after 40 abrasion cycles.

The WCA was evaluated after heating the mesh to assess its wetting behaviour. The WCA dropped with temperature, reaching 133.5 ± 2 ° when the heating temperature was raised to 200 °C. The mesh exhibited a WCA of 152 ± 2° at 150 °C heating, and the water drops on heated OPS-2 mesh are shown in Fig. 8(d). The thermal stability of the mesh was tested by dumping hot water at 97 ± 2 °C. As seen in Fig. 8(c), the hot water droplets had a spherical form on mesh. As a consequence, the produced coated mesh retains its superhydrophobic feature and separates hot water and oil combination.

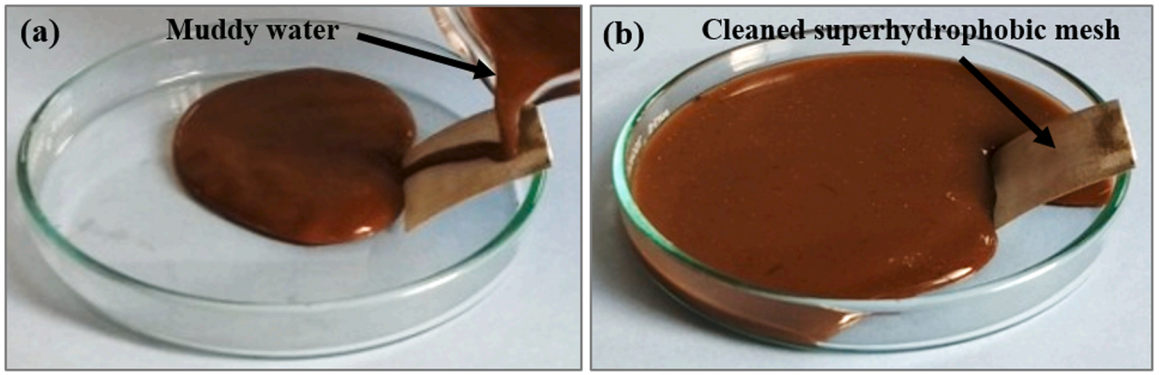

Fig. 9. Photographs of self-cleaning performance of OPS-2 mesh.

3.5. Self-cleaning performance

When used in an outdoor setting, accumulated dirt contamination, such as dust particles from the environment and sludge formed by the mixing of oil and water, may cause damage to the surface structure of the coating and lower its performance. The capacity of superhydrophobic coatings to clear themselves of dust particles without the need for additional pressures from the outside is one of the most remarkable characteristics of these coatings [54]. As a result, the dirt that has gathered on the superhydrophobic mesh is very simple to wash away using the jet of water. In this case muddy water, fine particles of ash and wood charcoal are used as dust containments to test the self-cleaning ability of optimized superhydrophobic OPS-2 mesh. The muddy water was dumped onto an angled superhydrophobic OPS-2 mesh. On a surface that is superhydrophobic, muddy water behaves much like regular water and rolls downhill. The fact that this was achieved reveals that the superhydrophobic mesh that was created had amazing self-cleaning characteristics. The photographic evidence of the self-cleaning procedure may be seen in Fig. 9. Further the self-cleaning ability of superhydrophobic OPS-2 mesh was checked by dipping in the dispersion of ash in water. The OPS-2 mesh was immersed in prepared dispersion of ash and pulled out. There was no ash sludge seen adhered to the OPS-2 mesh as shown in Fig. S2. The water jet dropped onto the dispersed fine particles of wood charcoal on inclined superhydrophobic OPS-2 mesh. The water droplets roll in downward by collecting charcoal particles and left cleaned OPS-2 mesh as shown in Fig. S3. This proves that OPS-2 mesh revealed distinguished self-cleaning characteristics.

4. Conclusions

In conclusion, we have successfully fabricated superhydrophobic and superoleophilic SS mesh by depositing consecutive layers of polystyrene (PS) and octadecyltrichlorosilane (OTS) using an easy and inexpensive dip coating method. This allowed us to create a superhydrophobic and superoleophilic surface on the SS mesh. The WCA of $157.5 \pm 2^{\circ}$, the OCA of about 0°, and the rolling angle of $6 \pm 2^{\circ}$ were all attained by adjusting the concentration of OTS in successive layered deposition. The investigation with the SEM showed that there is a regular arrangement of microscale bumps and on its surface there are nanoscale folds, both of which promote superhydrophobicity. The capacity of coatings to separate oil and water was tested using a variety of mixtures of oil and water, such as petrol, diesel, kerosene, vegetable oil, and coconut oil. The experiment into oil-water separation indicated a separation efficiency of more than 97% and a permeation flux of 1689.189 L/(m^2h) for low viscosity oil. After being bent, twisted, and folded multiple times, as well as subjected to 20 cycles of tape peeling testing and 30 cycles of sandpaper abrasion testing, the superhydrophobic coated mesh demonstrated that it maintained its superhydrophobic property throughout the duration of the mechanical durability study. Additionally, the superhydrophobic mesh that was created demonstrated exceptional thermal stability and good self-cleaning capabilities. As a consequence of this, the superhydrophobic mesh is an excellent choice for implementation on a wide scale in the oil-water separation process.

CRediT authorship contribution statement

Rajaram S. Sutar: Conceptualization, Methodology, Investigation, Writing – original draft, Writing – review & editing, **Sanjay S. Latthe:** Supervision, Writing – review & editing, Visualization, **Nilam B. Gharge:** Methodology, **Pradip P. Gaikwad:** Methodology, Investigation, **Akshay R. Jundle:** Methodology, Investigation, **Sagar S. Ingole:** Methodology, Investigation, **Rutuja A. Ekunde:** Methodology, **Saravanan Nagappan:** Formal analysis, Writing – review & editing, **Kang Hyun Park:** Validation, Investigation, **Appasaheb K. Bhosale:** Validation, Formal analysis, Investigation, **Shanhu Liu:** Supervision.

Declaration of Competing Interest

The authors declare that they have no known competing financial interests or personal relationships that could have appeared to influence the work reported in this paper.

Data availability

Data will be made available on request.

Acknowledgement

This work is financially supported by DST – INSPIRE Faculty Scheme, Department of Science and Technology (DST), Govt. of India. [DST/INSPIRE/04/2015/000281].

Appendix A. Supporting information

Supplementary data associated with this article can be found in the online version at doi:10.1016/j.colsurfa.2022.130561.

References

[1] M.W. Lee, S. An, S.S. Latthe, C. Lee, S. Hong, S.S. Yoon, Electrospun polystyrene nanofiber membrane with superhydrophobicity and superoleophilicity for selective separation of water and low viscous oil, ACS Appl. Mater. Interfaces 5 (21) (2013) 10597–10604.
[2] S. L Liu, Q. Xu, S.S. Latthe, A.B. Gurav, R. Xing, Superhydrophobic/superoleophilic magnetic polyurethane sponge for oil/water separation, Rsc Adv. 5 (84) (2015) 68293–68298.
[3] Y. Liu, K. Zhang, W. Yao, J. Liu, Z. Han, L. Ren, Bioinspired structured superhydrophobic and superoleophilic stainless steel mesh for efficient oil-water separation, Colloids Surf. A: Physicochem. Eng. Asp. 500 (2016) 54–63.
[4] S. Nagappan, C.-S. Ha, Emerging trends in superhydrophobic surface based magnetic materials: fabrications and their potential applications, J. Mater. Chem. A 3 (7) (2015) 3224–3251.
[5] S. Nagappan, J.J. Park, S.S. Park, W.K. Lee, C.S. Ha, Bio-inspired, multi-purpose and instant superhydrophobic–superoleophilic lotus leaf powder hybrid micro–nanocomposites for selective oil spill capture, J. Mater. Chem. A 1 (23) (2013) 6761–6769.
[6] M. Bennett, R.A. Williams, Monitoring the operation of an oil/water separator using impedance tomography, Miner. Eng. 17 (5) (2004) 605–614.
[7] B. Li, X. Liu, X. Zhang, J. Zou, W. Chai, J. Xu, Oil-absorbent polyurethane sponge coated with KH-570–modified graphene. J. Appl. Polym. Sci. 132 (2015) 16.
[8] C.H. Peterson, S.D. Rice, J.W. Short, D. Esler, J.L. Bodkin, B.E. Ballachey, D. B. Irons, Long-term ecosystem response to the Exxon Valdez oil spill, Science 302 (5653) (2003) 2082–2086.
[9] B. Chen, T. Wada, H. Yabu, Amphiphilic perforated honeycomb films for gravimetric liquid separation, Adv. Mater. Interfaces 9 (1) (2022), 2101954.
[10] Y. Wei, H. Qi, X. Gong, S. Zhao, Specially wettable membranes for oil–water separation, Adv. Mater. Interfaces 5 (23) (2018), 1800576.
[11] Y. Deng, C. Peng, M. Dai, D. Lin, I. Ali, S.S. Alhewairini, I. Naz, Recent development of super-wettable materials and their applications in oil-water separation, J. Clean. Prod. 266 (2020), 121624.
[12] S.S. Latthe, R.S. Sutar, A.K. Bhosale, K.K. Sadasivuni, S. Liu, Superhydrophobic surfaces for oil-water separation, in. Superhydrophobic Polymer Coatings, Elsevier, 2019, pp. 339–356.
[13] S. Rasouli, N. Rezaei, H. Hamedi, S. Zendehboudi, X. Duan, Superhydrophobic and superoleophilic membranes for oil-water separation application: a comprehensive review, Mater. Des. 204 (2021), 109599.
[14] E.K. Sam, J. Liu, X. Lv, Surface engineering materials of superhydrophobic sponges for oil/water separation: a review, Ind. Eng. Chem. Res. 60 (6) (2021) 2353–2364.
[15] Y. Liu, B. Zhan, K. Zhang, C. Kaya, T. Stegmaier, Z. Han, L. Ren, On-demand oil/water separation of 3D Fe foam by controllable wettability, Chem. Eng. J. 331 (2018) 278–289.
[16] R. Liao, Z. Zuo, C. Guo, Y. Yuan, A. Zhuang, Fabrication of superhydrophobic surface on aluminum by continuous chemical etching and its anti-icing property, Appl. Surf. Sci. 317 (2014) 701–709.
[17] C. Li, B. Lee, C. Wang, A. Bajpayee, L.D. Douglas, B.K. Phillips, L. Fang, Photopolymerized superhydrophobic hybrid coating enabled by dual-purpose tetrapodal ZnO for liquid/liquid separation, Mater. Horiz. 9 (1) (2022) 452–461.
[18] H.S. Hwang, N.H. Kim, S.G. Lee, D.Y. Lee, K. Cho, I. Park, Facile fabrication of transparent superhydrophobic surfaces by spray deposition, ACS Appl. Mater. Interfaces 3 (7) (2011) 2179–2183.
[19] W. Ma, Z. Jiang, T. Lu, R. Xiong, C. Huang, Lightweight, elastic and superhydrophobic multifunctional nanofibrous aerogel for self-cleaning, oil/water separation and pressure sensing, Chem. Eng. J. 430 (2022), 132989.

[20] Y. Wan, M. Chen, W. Liu, X. Shen, Y. Min, Q. Xu, The research on preparation of superhydrophobic surfaces of pure copper by hydrothermal method and its corrosion resistance, Electrochim. Acta 270 (2018) 310–318.
[21] H. Guo, J. Yang, T. Xu, W. Zhao, J. Zhang, Y. Zhu, L. Zhang, A robust cotton textile-based material for high-flux oil–water separation, ACS Appl. Mater. Interfaces 11 (14) (2019) 13704–13713.
[22] Y. Xiu, D.W. Hess, C.P. Wong, UV and thermally stable superhydrophobic coatings from sol–gel processing, J. Colloid Interface Sci. 326 (2) (2008) 465–470.
[23] Z. Xu, D. Jiang, Z. Wei, J. Chen, J. Jing, Fabrication of superhydrophobic nano-aluminum films on stainless steel meshes by electrophoretic deposition for oil-water separation, Appl. Surf. Sci. 427 (2018) 253–261.
[24] X.Q. Cheng, Y. Jiao, Z. Sun, X. Yang, Z. Cheng, Q. Bai, L. Shao, Constructing scalable superhydrophobic membranes for ultrafast water–oil separation, ACS nano 15 (2) (2021) 3500–3508.
[25] A.B. Radwan, A.M. Mohamed, A.M. Abdullah, M.A. Al-Maadeed, Corrosion protection of electrospun PVDF–ZnO superhydrophobic coating, Surf. Coat. Technol. 289 (2016) 136–143.
[26] L. Zhang, H. Chen, J. Sun, J. Shen, Layer-by-layer deposition of poly (diallyldimethylammonium chloride) and sodium silicate multilayers on silica-sphere-coated substrate—facile method to prepare a superhydrophobic surface, Chem. Mater. 19 (4) (2007) 948–953.
[27] S.S. Latthe, A.L. Demirel, Polystyrene/octadecyltrichlorosilane superhydrophobic coatings with hierarchical morphology, Polym. Chem. 4 (2) (2013) 246–249.
[28] D. Liu, Y. Yu, X. Chen, Y. Zheng, Selective separation of oil and water with special wettability mesh membranes, RSC Adv. 7 (21) (2017) 12908–12915.
[29] B. Zhou, B.H. Bashir, Y. Liu, B. Zhang, Facile construction and fabrication of a superhydrophobic copper mesh for ultraefficient oil/water separation, Ind. Eng. Chem. Res. 60 (22) (2021) 8139–8146.
[30] K.Y. Eum, I. Phiri, J.W. Kim, W.S. Choi, J.M. Ko, H. Jung, Superhydrophobic and superoleophilic nickel foam for oil/water separation, Korean J. Chem. Eng. 36 (8) (2019) 1313–1320.
[31] B. Pang, H. Liu, P. Liu, H. Zhang, G. Avramidis, L. Chen, K. Zhang, Robust, easy-cleaning superhydrophobic/superoleophilic copper meshes for oil/water separation under harsh conditions. Adv. Mater. Interfaces 6 (11) (2019), 1900158.
[32] B. Sun, F. Zhang, M. Gao, S. Zhao, J. Wang, W. Zhang, J. Wang, Superhydrophilic stainless steel mesh for oil–water separation with long-term durability, impressive corrosion resistance, and abrasion resistance, Adv. Eng. Mater. 22 (8) (2020), 2000262.
[33] X. Yue, D. Fu, T. Zhang, D. Yang, F. Qiu, Superhydrophobic stainless-steel mesh with excellent electrothermal properties for efficient separation of highly viscous water-in-crude oil emulsions, Ind. Eng. Chem. Res. 59 (40) (2020) 17918–17926.
[34] J. Li, Z. Zhao, Y. Zhang, M. Li, Z. Luo, L. Luo, Facile fabrication of superhydrophobic SiO_2*-coated mesh used for corrosive and hot water/oil separation.* J. Sol. -Gel Sci. Technol. 82 (1) (2017) 299–307.
[35] F. Liu, M. Ma, D. Zang, Z. Gao, C. Wang, Fabrication of superhydrophobic/superoleophilic cotton for application in the field of water/oil separation, Carbohydr. Polym. 103 (2014) 480–487.
[36] N. Lv, X. Wang, S. Peng, L. Luo, R. Zhou, Superhydrophobic/superoleophilic cotton-oil absorbent: preparation and its application in oil/water separation, RSC Adv. 8 (53) (2018) 30257–30264.
[37] Q. Ke, Y. Jin, P. Jiang, J. Yu, Oil/water separation performances of superhydrophobic and superoleophilic sponges, Langmuir 30 (44) (2014) 13137–13142.
[38] L. Liang, Y. Xue, Q. Wu, Y. Dong, X. Meng, Self-assembly modification of polyurethane sponge for application in oil/water separation, RSC Adv. 9 (69) (2019) 40378–40387.
[39] Q. Ke, G. Li, Y. Liu, T. He, X.M. Li, Formation of superhydrophobic polymerized n-octadecylsiloxane nanosheets, Langmuir 26 (5) (2010) 3579–3584.
[40] C. Ma, Y. Li, P. Nian, H. Liu, J. Qiu, X. Zhang, Fabrication of oriented metal-organic framework nanosheet membrane coated stainless steel meshes for highly efficient oil/water separation, Sep. Purif. Technol. 229 (2019), 115835.
[41] H. Li, G. Zhu, Y. Shen, Z. Han, J. Zhang, J. Li, Robust superhydrophobic attapulgite meshes for effective separation of water-in-oil emulsions, J. Colloid Interface Sci. 557 (2019) 84–93.
[42] J. Dai, L. Wang, Y. Wang, S. Tian, X. Tian, A. Xie, J. Pan, Robust nacrelike graphene oxide–calcium carbonate hybrid mesh with underwater superoleophobic property for highly efficient oil/water separation, ACS Appl. Mater. Interfaces 12 (4) (2020) 4482–4493.
[43] S.S. Latthe, R.S. Sutar, T.B. Shinde, S.B. Pawar, T.M. Khot, A.K. Bhosale, S. Liu, Superhydrophobic leaf mesh decorated with SiO_2 nanoparticle–polystyrene nanocomposite for oil–water separation. ACS Appl. Nano Mater. 2 (2) (2019) 799–805.
[44] Y. Jiang, C. Liu, Y. Li, A. Huang, Stainless-steel-net-supported superhydrophobic COF coating for oil/water separation, J. Membr. Sci. 587 (2019), 117177.
[45] H. Cao, W. Gu, J. Fu, Y. Liu, S. Chen, Preparation of superhydrophobic/oleophilic copper mesh for oil-water separation, Appl. Surf. Sci. 412 (2017) 599–605.
[46] Y. Hou, Z. Peng, J. Liang, S. Fu, Facile preparation of petaliform-like superhydrophobic meshes via moisture etching for oil-water separation, Surf. Coat. Technol. 399 (2020), 126124.
[47] B. Jiang, H. Zhang, L. Zhang, Y. Sun, L. Xu, Z. Sun, H. Yang, Novel one-step, in situ thermal polymerization fabrication of robust superhydrophobic mesh for efficient oil/water separation, Ind. Eng. Chem. Res. 56 (41) (2017) 11817–11826.
[48] H. Cao, J. Fu, Y. Liu, S. Chen, Facile design of superhydrophobic and superoleophilic copper mesh assisted by candle soot for oil water separation, Colloids Surf. A: Physicochem. Eng. Asp. 537 (2018) 294–302.
[49] X. Zeng, S. Xu, P. Pi, J. Cheng, L. Wang, S. Wang, X. Wen, Polymer-infiltrated approach to produce robust and easy repairable superhydrophobic mesh for high-efficiency oil/water separation, J. Mater. Sci. 53 (14) (2018) 10554–10568.
[50] X. Yin, Z. Wang, Y. Shen, P. Mu, G. Zhu, J. Li, Facile fabrication of superhydrophobic copper hydroxide coated mesh for effective separation of water-in-oil emulsions, Sep. Purif. Technol. 230 (2020), 115856.
[51] J. Huang, M. Li, Y. Lu, C. Ren, S. Wang, Q. Wu, X. Liu, A facile preparation of superhydrophobic L-CNC-coated meshes for oil–water separation, RSC Adv. 11 (23) (2021) 13992–13999.
[52] P. Varshney, D. Nanda, M. Satapathy, S.S. Mohapatra, A. Kumar, A facile modification of steel mesh for oil–water separation, N. J. Chem. 41 (15) (2017) 7463–7471.
[53] Z. Luo, Y. Li, C. Duan, B. Wang, Fabrication of a superhydrophobic mesh based on PDMS/SiO_2 nanoparticles/PVDF microparticles/KH-550 by one-step dip-coating method. RSC Adv. 8 (29) (2018) 16251–16259.
[54] A.M. Kokare, R.S. Sutar, S.G. Deshmukh, R. Xing, S. Liu, S.S. Latthe, ODS–modified TiO_2 nanoparticles for the preparation of self-cleaning superhydrophobic coating. in *AIP Conference Proceedings*, AIP Publishing LLC,, 2018.